journal

J. Am. Ceram. Soc., 95 [10] 3239–3245 (2012)
DOI: 10.1111/j.1551-2916.2012.05311.x

Stoichiometry and Grain Boundaries Control by Spark Plasma Sintering in $Ba_{0.6}Sr_{0.4}TiO_3$:Mn/MgO Composites

Catherine Elissalde,[‡,†] U-Chan Chung,[‡] Alla Artemenko,[‡] Claude Estournès,[§] Romain Costes,[¶] Michel Paté,[¶] Jean-Pierre Ganne,[¶] Sabine Waechter,[‖] and Mario Maglione[‡]

[‡]CNRS, Université Bordeaux I, ICMCB, 87 Av. Dr. A. Schweitzer, 33608 Pessac, France

[§]CIRIMAT et Plateforme Nationale CNRS de Frittage Flash, PNF2 MHT, Université Paul Sabatier, 33062 Toulouse, France

[¶]Thales Research and Technology, 1 Av. Augustin Fresnel, 91767 Palaiseau Cedex, France

[‖]Julius-Maximilians Würzburg University, Sanderring 2, D-97070 Würzburg, Germany

This study highlights the possibility to control materials' chemistry simultaneously at the atomic and micrometric scales and to design functional oxide-based multimaterials, thanks to the specificity of Spark Plasma Sintering (SPS). We have used a dual synthesis route, namely chemical and composite, combined with SPS to adjust the oxidation state of intrinsic and dopant ions, the grain boundaries state, and to control interdiffusion in composites made of Mn-doped $Ba_{0.6}Sr_{0.4}TiO_3$ (BST) and MgO. At the atomic level, the Mn substituent valence state can be fixed according to the sintering process: Electron Paramagnetic Resonance evidenced Mn_{Ti}^{2+}, Mn_{Ti}^{4+}, and Mn_{Ti}^{2+}-V_O charged defects. We established a link between the nature of the charged defects and the high-frequency dielectric losses. At the microscopic level, control of the grain size, the grain boundaries, and the interdiffusion between the components is achievable using SPS. The composite effect acts at low frequency by efficiently decreasing the extrinsic losses arising from the grain boundaries contribution and by increasing the thermal stability of the permittivity. Such an approach based on SPS, chemical and composite routes, has allowed designing BST-based composites operating in a wide frequency range (kHz–GHz) with low dielectric losses and high electric field tunability.

I. Introduction

Integration of ferroelectric materials in electronic devices always calls for the design of agile components i.e. with electric characteristics variable as a function of an external electric field. The current trend aims to develop multifunctional, low cost, and small dimensional materials with high performance. Ferroelectric materials are dielectric materials for which the dielectric permittivity, ε, can be significantly and reversibly tuned by an electric field. The tunability is defined as follows: $A\ (\%) = |\varepsilon\ (T,\ E) - \varepsilon\ (T,\ E = 0)|\ /\varepsilon\ (T, E = 0) \times 100$, where E is the electric field and T the temperature. This functionality can be applied to emission, reception, as well as signals processing that require electronic components (antennas, filters, frequency tunable oscillators, …), which are likely to simultaneously manage several frequencies in everyday telecommunication. To answer this need of flexibility, capacitors with adjustable capacity through a low electric voltage are a promising option. Tunable capacitors can replace several capacitors with fixed capacitance, thus offering significant perspectives of reduction in size of devices.

To allow electromagnetic waves management, the ideal material requires specific properties: (i) moderate permittivity values, (ii) low dielectric losses ($\leq 1\%$) in a wide frequency range (from kHz up to GHz), (iii) good thermal stability, and (iv) high tunability of the dielectric susceptibility (>10%). However, all these characteristics are hardly met in standard materials mainly because the reduction of losses requires a smearing out of the ferroelectric behavior, which in turn alters the dielectric tunability.[1–3] To comply with this intrinsic contradiction and to improve the overall behavior of ferroelectric ceramics, two complementary routes have been used till now: (i) the composite one, based on the mixing between a ferroelectric $Ba_{1-x}Sr_xTiO_3$ (BST) phase and a low losses dielectric material like MgO[4–9]; (ii) the chemical one, with the substitution on the ferroelectric active Ti site of BST by cations like Mn.[10–15] Although a wealth of composites and substitutions have been attempted during the past 15 yrs, the property control toward the optimization of the relative contribution of both routes has not yet been achieved. The main reason is that, using standard sintering, only a restricted control of the materials chemistry (chemical interdiffusion at the grain boundaries, oxygen deficiency, dopant, and intrinsic charged defects valence state) is possible.

We show here that the use of SPS makes possible the merging between the two aforementioned routes, thus allowing the designing of materials chemistry simultaneously at the microscopic and atomic scales. SPS not only allows obtaining high densification but also reduces the interdiffusion between composite components ($Ba_{1-x}Sr_xTiO_3$ and MgO) and fixes the oxidation state of intrinsic and substituting ions. This is shown by comparison of ceramics obtained by conventional sintering and SPS. Thanks to complementary Electron Paramagnetic Resonance (EPR) investigations, we show how the oxidation state and the local environment of manganese ions directly impact composites' dielectric properties. In particular we demonstrate nonhomogeneous Mn-ions distribution within BST grains, which are acting like traps for charge carriers decreasing high-frequency dielectric losses. Finally, thanks to SPS, we are able to combine the positive effects of both the composite and the substitution routes and to obtain functional ceramics with high thermal stability, low dielectric losses in a wide frequency range (kHz–GHz) while keeping high electric field tunability.

II. Experimental Procedure

(1) Materials and Sintering Process

$Ba_{0.6}Sr_{0.4}TiO_3$ powders (average grain size 50 nm) used for BST/MgO composites were purchased from Pi-Kem (Tilley,

C. Randall—contributing editor

Manuscript No. 30475. Received October 14, 2011; approved May 04, 2012.
†Author to whom correspondence should be addressed. e-mail: elissald@icmcb-bordeaux.cnrs.fr

U.K.) and MgO (97%) was supplied by Merck (Darmstadt, Germany).

$Ba_{0.6}Sr_{0.4}TiO_3$ doped with 1 mol% Mn was prepared by solid-state reaction using $BaCO_3$ (Merck, 99%), $SrCO_3$ (Merck, 99%), $MnCO_3$ (Merck, 99%), and TiO_2 (Merck, 99%) precursors. The raw powders were ball-milled in stoichiometric proportions in a jar with zirconia balls for 2 h in an aqueous medium. The slurry was dried in an oven at 90°C overnight. The mixture was calcinated during 2 h either at 1275°C or 1150°C to prepare, respectively, micrometer (average grain size 1 μm) and submicrometer (large grain size distribution ranging from 50 to 300 nm) green powders. Powders were then ground for 2 h in alcohol.

Micrometric 1 mol% Mn-doped $Ba_{0.6}Sr_{0.4}TiO_3$ powder was shaped into pellets (6-mm diameter and 1-mm thickness) and uniaxially pressed. Standard sintering was performed in a Nabertherm (Bremen, Germany) RHTC 40-450/15 tubular furnace at 1400°C during 2 h (heating rate of 100°C/h) with two additional steps at 250°C and 600°C of 1 h each, under oxygen atmosphere.

The 1 mol% Mn-doped $Ba_{0.6}Sr_{0.4}TiO_3$ and all the composites (BST/MgO and Mn-doped BST/MgO) were sintered using Spark Plasma Sintering apparatus (Dr Sinter SPS-2080 SPS Syntex INC Japan of the Plateforme Nationale de Frittage Flash (PNF2) of CNRS located in Toulouse (France). Powders (without any sintering aids) were loaded onto a cylindrical die of 8-mm inner diameter. The pulse sequence was 12-2 (pulses-dead time or zero current) as recommended by the constructor. The temperature was raised to 600°C over a period of 3 min, and from this point it was monitored and regulated by an optical pyrometer focussed on a small hole located at the surface of the die. A heating rate of 100°C/min was used to reach the final temperature of 1200°C under vacuum. Uniaxial pressure of either 50 or 100 MPa was applied immediately before and until completion of the temperature rising step. The as-obtained SPS ceramics were reoxidized during a postthermal treatment performed in air at 800°C for 12 h.

(2) Microstructural and Dielectric Characterizations

Microstructural characterizations were performed using a Scanning Electron Microscope JEOL JSM 6360A (Cruissy-sur-Seine, France) and a High-Resolution Scanning Electron Microscope JEOL 6700F. A thin Au/Pd coating was deposited onto the ceramics fracture surface prior to observation.

Dielectric measurements were performed on discs using a Wayne-Kerr (West Sussex, England) component analyzer 6425 for temperatures between 200 and 500 K, and in the frequency range 100 Hz–100 kHz. Gold electrodes were sputtered on the circular faces of the dense compacts prior to measurements.

Measurements of permittivity in the GHz region were done using the method developed by Hakki and Coleman.[16] The sample of a cylindrical shape was placed between two metal plates. Under these conditions, the resonance frequency depends only on its permittivity and dimensions, and therefore can be analytically calculated. Microwave signal was applied and detected by two coupling loops linked to a voltage network analyzer (Agilent N5230C; Agilent Technologies France, Massy, France).

For losses measurements, the cylinder was placed between the same loops, separated from the lower metallic plate by lossless foam to eliminate the metallic losses. To avoid radiation losses, a cylindrical shield was placed around the resonator. Under such conditions, quality factor of the material equals to the measured quality factor of the resonator.

The tunability was measured applying to the sample, a static field of 1 kV/mm using a high voltage supply (Bertan Series 225; Spellman High voltage Electronics Corporation, Hauppauge, NY). A homemade decoupling device was used to protect the impedance meter from the bias. To avoid breakdown in the air (~1000 V), the sample was put in a bath of silicone oil.

(3) Electron Paramagnetic Resonance (EPR)

Electron Paramagnetic Resonance measurements were performed using X-band Bruker spectrometer (Karlsruhe, Germany), operating at a frequency of 9.4 GHz. An Oxford Instruments (Oxford, U.K.) ESR 9 He cryostat operating in the temperature range 4–300 K was used for temperature dependence of EPR spectra intensities studies.

III. Results and Discussion

To discriminate between the individual contribution of each route (composite and chemical), we analyze them first separately [Sections III*(1)* and *(2)* respectively] and then only together [Section III*(3)*]. In all cases, the bulk composites were sintered using SPS, starting from mixtures of $Ba_{0.6}Sr_{0.4}TiO_3$ (hereafter referred as BST) and MgO powders.

We have shown in previous work that SPS allows reaching high final ceramics density with limited interdiffusion between the two components.[17,18] These two conditions are crucial to propose a reliable comparative dielectric study. This is not a trivial concern as usually BST/MgO sintering requires high temperatures (>1400°C) due to the refractory character of MgO and leads to unavoidable interdiffusion leading to a decrease of the ferroelectric transition temperature.[5–9,19,20] Thanks to SPS, the sintering temperature can be lowered down to 1200°C while obtaining density higher than 95% for all composites.

(1) Composite Route: Influence of MgO Content on BST/MgO Composites Properties

$Ba_{1-x}Sr_xTiO_3$ (BST) nanoparticles were mixed with different MgO powder contents from 0 to 10 wt% (noted BST/10MgO) and sintered by SPS at 1200°C. The thermal evolution of the permittivity measured at 10 kHz shows that the value of T_C for the SPS composites is the same as for the pure BST sintered under the same conditions [Fig. 1(a)]. This is unambiguous evidence that whatever the MgO content, no interdiffusion occurred in SPS composites. As expected, the higher is the MgO content, the larger is the decrease in permittivity; the transition peak becomes more depressed, and even very diffuse for the composite BST/10MgO. At room temperature and at 10 kHz, the dielectric losses are strongly decreased reaching values as low as 0.002 (BST/10MgO) [Fig. 1(b)]. Whatever the MgO content, we obtain similar microstructures made of a BST matrix and long plate-like inclusions containing hundreds of grains of MgO [Fig. 1(b), inset]. The interfaces are very clean without any delamination or cracks. Two particle sizes are observed in the BST matrix, depending on whether they are close to the MgO clusters (nanosize grains) or not (grain size up to few micrometers). The plate-like shape of the inclusions results from the uniaxial pressure applied during the SPS process, leading to the crushing of the MgO agglomerates. A 3-D imaging approach and numerical simulation by Discrete Element Method are actually in progress to correlate the effective properties of the composites with their microstructure. This will be the first step toward reliable modeling of the dielectric properties. For the dielectric study, the electrodes were deposited parallel to the large MgO clusters surfaces. The tunability of the permittivity with the electric field was evaluated at 100 kHz, applying an electric field of 1 kV/mm in a direction perpendicular to the dielectric inclusions larger dimension (MgO). The tunability dramatically decreases down to 4% for BST/10MgO whereas 25% was obtained for BST/4MgO, a value comparable to that of pure BST.[18] Microwave measurements in the GHz range gave dielectric losses close to 0.04, both for the pure BST and for the composites containing either

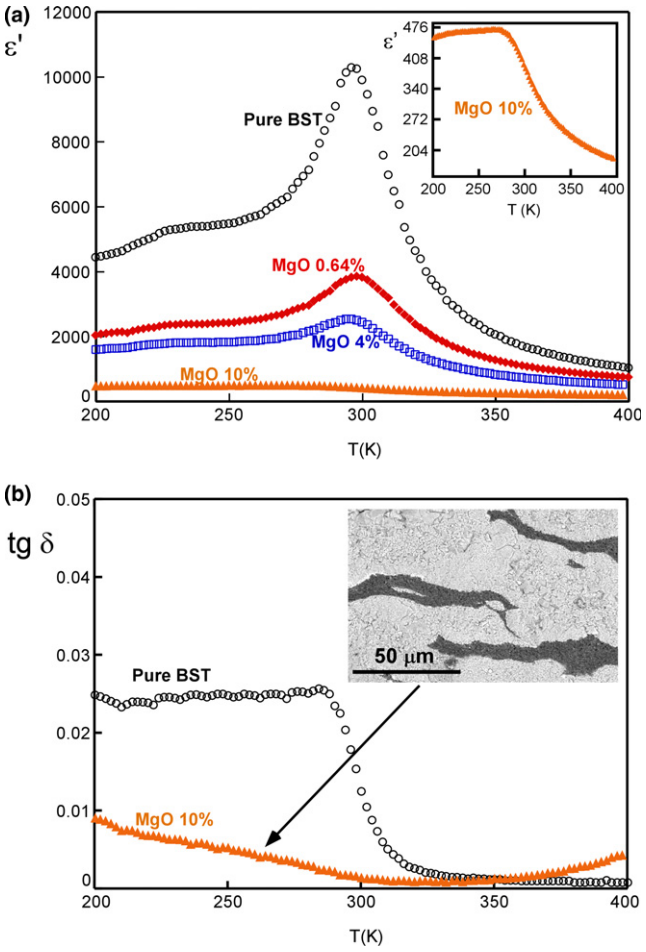

Fig. 1. Thermal variations of (a) dielectric permittivity and (b) losses at 10 kHz of Spark Plasma Sintered BST mixed with various contents of MgO (0, 0.64, 4, and 10 wt%). (Inset 1a) Zoom on the thermal variation of dielectric permittivity of BST-10%MgO composite. (Inset 1b) SEM chemical contrast micrograph of the fracture of 3-D random BST- 10%MgO composite sintered by SPS; dark areas correspond to MgO inclusions within the BST matrix.

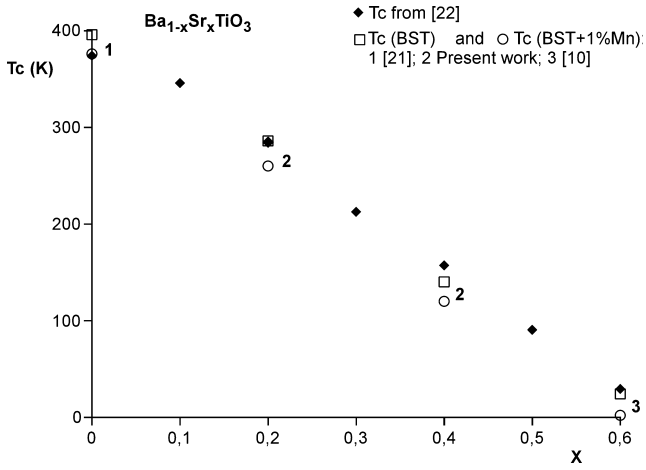

Fig. 2. T_C values of $Ba_{1-x}Sr_xTiO_3$ ceramics (♦ from [22] and □ from [21, 10] and this work) and T_C values of $Ba_{1-x}Sr_xTiO_3$: 1 mol% Mn ceramics (○ from [21, 10] and this work) as a function of Sr content. Error bars are not noted for sake of clarity, but would be added as T_C values depends on synthesis and sintering methods. However, the main information we demonstrate refers to the constant shift of 10 K from T_C (BST) to T_C (BST:Mn) for ceramics obtained by different research groups.

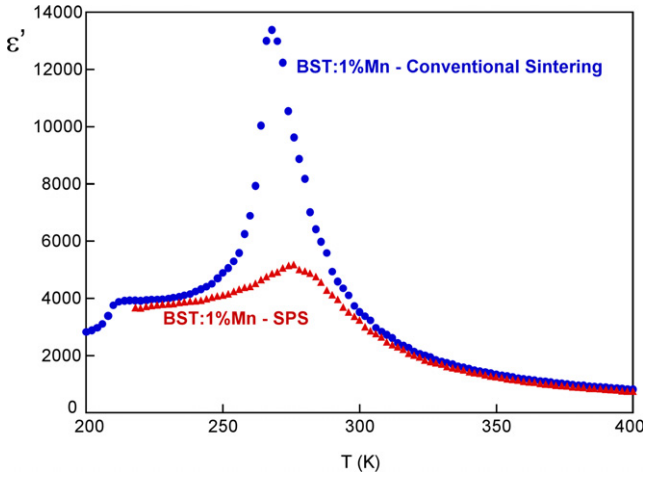

Fig. 3. Thermal variations of dielectric permittivity at 10 kHz of BST:1%Mn obtained by (•) conventional sintering and (▲) Spark Plasma Sintering.

0.64 or 4 wt% MgO. Only a slight decrease of dielectric losses from 0.04 to 0.03 was obtained when the dielectric phase content is increased up to 10 wt%. This comparative study evidences that increasing MgO content does not allow decreasing the high-frequency dielectric losses, which remain similar to that of pure BST. As a result, a composite containing 4% MgO content was selected in the following to guarantee sufficiently high tunability while achieving moderate low-frequency losses. To improve the high-frequency properties, the chemical route was investigated using manganese substitution and was tested in a first step on pure BST.

(2) Chemical Route: Manganese-Doped BST

(A) Effect of the Substitution on the Dielectric Characteristics of BST: The effect of Mn doping on reducing the high-frequency dielectric losses of $BaTiO_3$ is now well established.[13,21] The main role of manganese as a substituent of titanium is to trap the electrons produced by the creation of oxygen vacancies during sintering. This is still ascribed as the principal mechanism for decrease of losses. However, the change of the Curie temperature (T_C) resulting from Mn doping has to be considered for properties control. We are reporting on Fig. 2 different data from literature and our own results to probe as a function of the Ba/Sr ratio the effect of 1%Mn doping on the Curie temperature.[10,21,22] The effect of a 1 mol% Mn substitution results in a systematic decrease of T_C by 10 K as compared to pure BST, whatever the Ba/Sr ratio (Fig. 2). At the low rate of Mn substitution used here, we can state that the shift of T_C resulting from the Mn/Ti substitution is the same for all the Ba/Sr ratios. This means that the disturbance of the octahedral B site is not coupled to the A-site one. The Curie temperature can be considered as a very accurate probe of the ferroelectric correlation.[23,24] Thus, we highlight that Mn substitution enables reduction of the microwave losses: (i) by trapping the excess charges and (ii) by scaling down the ferroelectric correlation, whereas the composite route does not allow such effect. An additional way to modify the ferroelectric correlation is to generate charged defects using specific conditions of sintering.

(B) Conventional Sintering versus SPS: Conventional sintering of 1 mol% Mn-doped BST (micrometer grain size green powder) was performed in air at 1400°C during 2 h. A sharp maximum of ε′ close to 14 000 at T_C was obtained (Fig. 3); the 1 GHz losses are strongly decreased (0.008) and the tunability measured under 1 kV/mm at 100 kHz is about 15%. Such dielectric characteristics for the conventional sintered sample are satisfying, but the thermal sensitivity of the ferroelectric anomaly remains a drawback for applications.

SPS treatment results in a drastic drop in the permittivity at T_C (max 5000) whereas the permittivity in the vicinity

of the second ferroelectric transition ($T \approx 215$ K) remains similar to that obtained by conventional sintering (4000) (Fig. 3). As a result, a significant stabilization of the permittivity is achieved in the whole investigated temperature range.

Such difference in permittivity cannot be ascribed to the density of the ceramics, which is similar and close to 95% in both conventional sintering and SPS cases. We have to discard a possible contribution of size effect as the grain size is larger when using conventional sintering (about 5 μm) and remains above 1 μm in the case of SPS.[25,26]

As SPS is performed under low oxygen partial pressure (vacuum) with subsequent reoxidation, the valence state of intrinsic and substituting ions appears as a critical point and may explain the different dielectric behavior observed depending on the sintering process. This possibility was probed using EPR and the results are detailed hereafter.

(C) EPR Characterization of the Defects: Electron Paramagnetic Resonance experiments were performed in a wide temperature range to determine the oxidation state of charged defects in the materials at different stages of their synthesis. The probed materials were the initial powder of $Ba_{0.6}Sr_{0.4}TiO_3$ substituted with 1% of Mn, the resulting sintered samples using both conventional sintering process and SPS. SPS samples were probed before and after reoxidation in air (thermal treatment at 800°C). Some of the spectra recorded at 4 K are shown in Fig. 4.

The spectra for the initial powder (not-shown) and the conventionally sintered sample can be divided in two regions with a broad signal at low magnetic field and a poorly resolved hyperfine set in the magnetic field range 3000–4000 G. The broad line is arising from some residuals of $MnCO_3$ precursor that were identified from the characteristic temperature dependence of the signal, as checked directly on $MnCO_3$ powders. This resonance evidences that only a part of the manganese could enter the structure, therefore lowering the intensity of the signal due to substituted Mn. Resonances marked by asterisk in Fig. 4 with $g = 2.0035$ and a hyperfine structure parameter $A = (82.6 \pm 0.2) \times 10^{-4}$ cm^{-1} are typical of Mn^{2+} ions in an octahedral environment and substituting Ti^{4+} ions in $BaTiO_3$ [BT] or $SrTiO_3$ [ST] single crystals and ceramics (average values are $g = 2.0025 \pm 0.001$ and the hyperfine structure parameter $A = (82.6 \pm 0.4) \times 10^{-4}$ cm^{-1}).[27–31] The low oxidation state can be understood from both the low concentration for this substituent and some unavoidable oxygen vacancies compensating for the charge excess. Note, however, that some EPR silent species like Mn^{3+} can still be present in the standard sintered sample.

As the SPS is performed under vacuum (i.e., low oxygen partial pressure), the creation of a relatively high concentration of oxygen vacancies as well as a change in the oxidation state of the intrinsic and substituting ions (Mn in our case) can be expected. In our case however, only an intensive Mn^{2+} resonance sextet was recorded. This spectrum is again attributed to Mn^{2+} ions substituting titanium ions (Mn_{Ti}^{2+}). The intensity of the spectrum is very high in comparison to the one observed for the sample after the conventional sintering and several reasons can be highlighted for that: (i) with the SPS sintering, no more traces of the initial carbonates can be observed, i.e. all manganese ions from initial $MnCO_3$ can be assumed to be incorporated in BST and participate to the signal; (ii) Mn_{Ti}^{2+} are obviously also compensated by oxygen vacancies; however, the short duration of the SPS prevents the establishment of the thermal equilibrium and discards a direct compensation in the nearest Mn sphere, i.e. impedes the creation of Mn_{Ti}^{2+}-V_O centers; (iii) some additional Mn^{2+} ions might further have been created from the reduction of some EPR-silent Mn^{3+}. It appears that the SPS treatment,

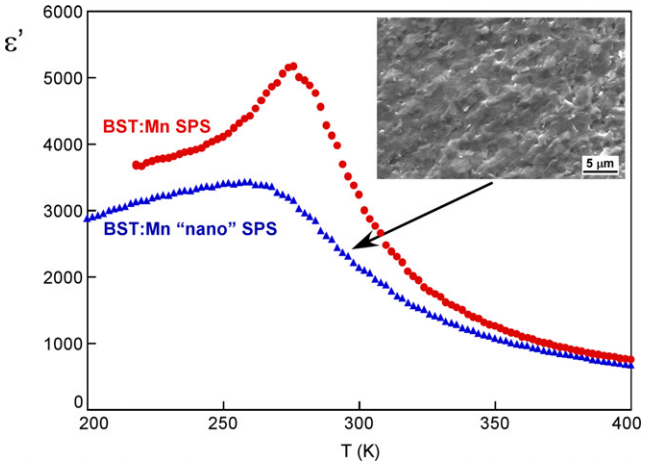

Fig. 5. Thermal variations of dielectric permittivity at 10 kHz of BST:1%Mn sintered by spark plasma sintering: ceramics obtained from (•) micrometric and (▲) nanometric initial powders (SEM micrograph of the fracture of the ceramic in inset).

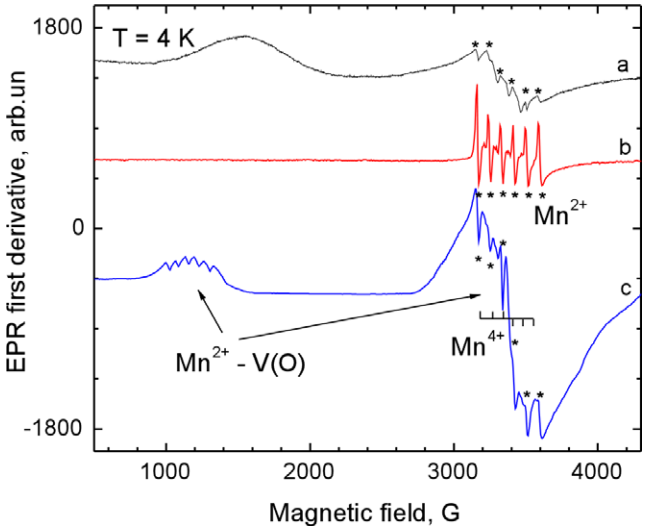

Fig. 4. EPR spectra recorded at 4 K: (a) $Ba_{0.6}Sr_{0.4}TiO_3$:1%Mn after conventional sintering; (b) $Ba_{0.6}Sr_{0.4}TiO_3$: 1%Mn SPS sintered; (c) $Ba_{0.6}Sr_{0.4}TiO_3$: 1%Mn SPS sintered with subsequent reoxidation. Sextet of resonance lines originated from Mn^{2+} substituted for Ti^{4+} is marked by asterisks.

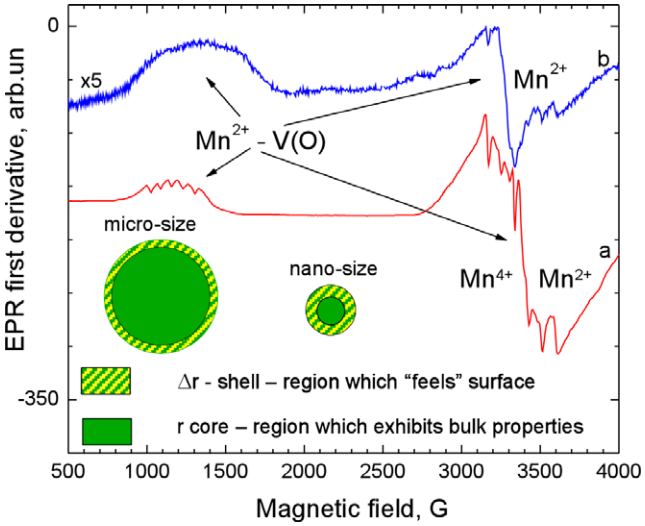

Fig. 6. EPR spectra recorded at 4 K for SPS sintered and reoxidized samples starting from (a) micro- and (b) nanosize Mn-doped BST powders. The scheme of core@shell architecture in the case of micro- and nanosize particles.

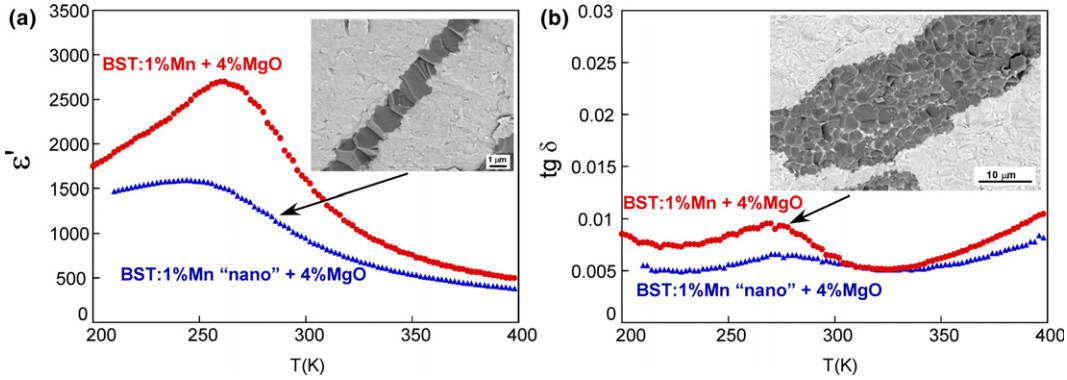

Fig. 7. Thermal variations of (a) dielectric permittivity (inset: SEM micrographs of the fracture of the composites) and (b) losses at 10 kHz of BST:1%Mn + 4%MgO composites sintered by spark plasma sintering: ceramics obtained from (•) micrometric and (▲) nanometric initial powders.

both with the reducing and the short time conditions, favors the creation of isolated Mn_{Ti}^{2+} defects in the titanium site.

SPS performed in vacuum can also lead to the Ti^{4+} reduction to Ti^{3+}. This last one is paramagnetic $3d^1$ ion with electron spin $S = 1/2$ and is visible from EPR, like we reported for the textured BT films.[32] No signal which could be ascribed to the reduced titanium Ti^{3+} ions was observed for SPS-sintered Mn-doped BST ceramics even at low temperatures, at which the ion is usually observed because of short spin-lattice relaxation time. These results reveal that during SPS sintering, substituting ions are preferentially changing their valence state, in our case $Mn^{4+/2+}$, impeding titanium ions from reduction ($Ti^{4+/3+}$).

Deep changes in the EPR spectra arise after the reoxidation, in air, of this last sample. In addition to the lines already present in the as-(SPS)-sintered sample (marked by asterisk in Fig. 4), new resonances appear (i) centered at 3350 G and (ii) in the low magnetic field region (800–1600 G). The spectra deconvolution allows separating two additional manganese-related paramagnetic centers: Mn^{4+} and Mn_{Ti}^{2+}-V_O. Mn^{4+} offers a typical cubic symmetry spectrum with isotropic g-factor and A values given by $g = 1.995$ and $A = (70.2 \pm 0.2) \times 10^{-4}$ cm^{-1}. Such centers with close parameters were already reported for Mn^{4+} ions substituting for Ti^{4+} in BT and ST host.[27] The second center (Mn_{Ti}^{2+}-V_O) is characterized by axial parameters with effective g-factor values $g_{//} = 2.002$ and $g_{\perp} = 5.85$. Such spectrum is attributed to transitions between the central $\pm 1/2$ ($\Delta M = \pm 1$) levels of Mn^{2+} ions located in a strong tetragonal crystalline field. In perovskite crystals, (e.g., BT or ST) the tetragonal crystalline field presumably arises from a nearest-neighbor oxygen vacancy, justifying the assignment to an axial Mn_{Ti}^{2+}-V_O defect. The influence of oxygen vacancies on properties of BT-based composites was revealed in our previous work.[33] The presence of such defects can be easily understood from the history of the sample: (i) after the SPS treatment, oxygen vacancies are created and (ii) for charge compensation, manganese is incorporated at the titanium site with +II oxidation state; (iii) the diffusion of the oxygen vacancies is hindered by the short-time reaction; (iv) the sample globally contains only isolated Mn^{2+} and V_O. The long annealing in air produces two effects: (i) it partly oxidizes Mn^{2+} into Mn^{4+} and (ii) it favors the mobility of a part of the oxygen vacancies toward the Mn^{2+} defects and promotes the creation of Mn_{Ti}^{2+}-V_O defects. The latter defect is a big static dipole, which breaks the ferroelectric correlation leading to a strong decrease of the dielectric permittivity, as compared to conventional sintered sample and as discussed in the previous section (Fig. 3).

(D) Influence of the Initial Grain Size: Spark Plasma Sintering was also performed starting from Mn-doped BST powder with nanometer initial grain size in the range 50–300 nm. Submicrometer grain size was preserved in the final ceramics (hereafter called nanoSPS) while maintaining density value higher than 95%. As compared to the ceramics obtained from a powder with micrometer initial grain size (hereafter called microSPS), T_C is decreased and the transition peak is more diffuse (Fig. 5).

The Mn ions substitution and its repartition within the grain can play a crucial role on these dielectric properties depending on its distribution in the bulk, at the grain boundaries or in a "core@shell" structure (in terms of chemically inhomogeneous structure) when the grain size is sufficiently small. EPR has already been shown to be a powerful tool to probe such chemical heterogeneities.[34–36] We thus used EPR on nanoSPS and microSPS ceramics to check the Mn gradients within each grain. From the comparison of EPR spectra reported on Fig. 6, several conclusions can be given: (i) resonances observed for the nanoSPS ceramics have the same origin as the ones for the microSPS ceramics and in particular, the low magnetic field resonance confirms the Mn_{Ti}^{2+}-V_O defects' presence; (ii) the lines broadening and the absence of resolved hyperfine structure for the nanoSPS sample is due to size effect; (iii) SPS and long-time (12 h) postsintering reoxidation in air leads to the oxygen ions mobility toward Mn^{2+} creation of the Mn_{Ti}^{2+}-V_O defects; (iv) manganese impurity ions are not randomly distributed within particles, but are concentrated at the surface and close region creating particles shell, in particular, in nanoSPS sample the Mn_{Ti}^{2+}-V_O defects are mainly concentrated at the surface of the grains; (v) as revealed by EPR, during postsintering reoxidation Mn^{2+} ions are partly changing their valence state to Mn^{4+}. From items (ii) and (iv), we conclude that the dielectric peak broadening in nanoSPS stems from the core-shell

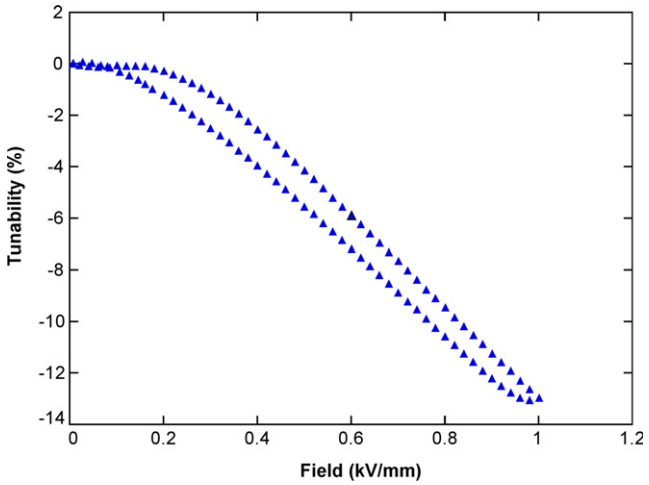

Fig. 8. Electric field tunability of the permittivity at 100 kHz in BST:1%Mn + 4%MgO composite sintered by SPS.

Table I. Comparison of Microstructural and Dielectric Characteristics of Different Composites Sintered by SPS

	BST	BST + 4%MgO	BST:1%Mn + 4%MgO	BST:1%Mn (nano) + 4%MgO
BST final grain size	5–10 μm	5–10 μm 200 nm–1 μm†	2 μm	500 nm–1 μm
MgO final grain size	–	300 nm	2 μm	2 μm
tan δ (300 K–10 kHz)	1%	0.5%	0.6%	0.55%
tan δ (300 K to ~1 GHz)	4%	4%	1.4%	1.25%
Tunability (%) (1 kV/mm–100 KHz)	25	25	13	3
Figure of Merit: Tunability/tan δ	6.25	6.25	9.28	2.4

BST Refers to the Composition $Ba_{0.6}Sr_{0.4}TiO_3$.
†Around MgO inclusions.

chemical heterogeneity whose contribution increases because of the size effect.

(3) Combination of Both Chemical and Composite Routes: Mn-Doped BST/MgO

To decrease the dielectric losses in a broad frequency range from kHz to GHz, the composite (addition of 4 wt% of MgO) and the chemical (1 mol% Mn doping) routes were combined. As discussed in Section III*(1)*, 4% of MgO content was selected on the basis of the best compromise between high tunability and moderate low-frequency losses. The dielectric properties of two different SPS ceramics were investigated starting from 1% Mn-doped BST powders with micro and nanometer initial grains size [Figs. 7(a) and (b)]. Chemically sharp interfaces are still observed between BST:1% Mn and MgO. A significant difference in the microstructure, in terms of both homogeneity and grain size, is observed whatever the BST:1% Mn initial grain size: the Mn doping of the BST leads to a homogeneous ferroelectric matrix contrary to the complex dual microstructure described in Section III *(1)*, indicating a possible grain-growth inhibition effect of Mn substitution. In addition, a significant MgO grain growth is observed within the agglomerates [inset Figs. 7(a) and (b)]. The low-frequency losses are below or close to 1% in the whole investigated temperature range [Fig. 7(b)]. The positive effect of Mn substitution on decreasing the high-frequency losses is maintained in the two different composites with a value dropping down to 0.014 at 1 GHz (instead of 0.04 in undoped BST/4%MgO). In addition, a tunability as high as 13% under 1 kV/mm was obtained (Fig. 8). Decrease of BST grains to nanosize affects the value of permittivity strongly and leads to a significant decrease in tunability, from 13% to 3% [Figs. 7(a) and (b)]. Such grain size effects are similar to that observed in the case of ceramics without MgO addition (decrease of the Curie temperature, permittivity, and losses).

Dielectric and microstructural characteristics of different composites sintered by SPS are listed in Table I. Comparing the figure of merit of the three composites BST + 4%MgO, BST:Mn + 4% MgO, and (nanosize) BST:Mn + 4% MgO, the second one appears as the best candidate for applications (characteristics of pure BST are given as reference).

IV. Conclusion

Spark Plasma Sintering was used to design, at the microscopic and atomic scales, composites made of $Ba_{0.6}Sr_{0.4}TiO_3$: Mn and MgO. Such a multiscale approach allowed optimizing the dielectric properties of BST (composition $Ba_{0.6}Sr_{0.4}TiO_3$) in broad frequency (kHz–GHz) and temperature ranges. We have shown that SPS allows interfaces control without interdiffusion between BST and MgO (up to 10 wt %). Addition of 4%MgO decreases the low-frequency dielectric losses while keeping high permittivity tunability. Combining the composite route with a chemical one, the substitution of Ti by Mn, allows further decreasing of the high-frequency dielectric losses. Manganese ions (Mn_{Ti}^{2+} and Mn_{Ti}^{4+})are breaking the long-range correlation along the Ti–O chains due to the change in the ionic radius and mass, and even more efficiently when using SPS by the creation of big Mn^{2+} - Vo charged defects as revealed from EPR measurements. Based on such controlled multiscale approaches, the composite made of BST:Mn + 4%MgO exhibits high tunability (13% under 1 kV/mm), low dielectric losses in a large frequency range and high thermal stability of the permittivity. This study highlights the advantage of SPS to act simultaneously at two different scales (atomic and microscopic) in a single material, allowing thus the design of functional oxide-based multimaterials with adjustable dielectric characteristics through the material chemistry control.

Acknowledgments

Financial support from the French National Center for Scientific Research (CNRS), the National Research Agency (ANR), and for EPR investigations, a Marie Curie International Incoming Fellowship within the 7th European Community Framework Programme (GA 255662), are gratefully acknowledged. The authors would thank G. Chevallier for spark plasma sintering assistance.

References

[1]A. K. Tagantsev, V. O. Sherman, K. F. Astafiev, J. Venkatesh, and N. Setter, "Ferroelectric Materials for Microwave Tunable Applications," *J. Electroceram.*, **11**, 5–66 (2003).
[2]V. O. Sherman, A. K. Tagantsev, N. Setter, D. Iddles, and T. Price, "Ferroelectric-Dielectric Tunable Composites," *J. Appl. Phys.*, **99**, 074104 (10pp) (2006).
[3]V. O. Sherman, A. K. Tagantsev, and N. Setter, "Model of a Low Permittivity and High Tunability Ferroelectric Based Composites," *Appl. Phys. Lett.*, **90**, 162901 (3pp) (2007).
[4]L. Sengupta, "Ceramic Ferroelectric Composite Material BSTO-Magnesium Based Compound"; Brevet U.S. 5635434, 1997.
[5]W. Chang and L. Sengupta, "MgO-Mixed $Ba_{0.6}Sr_{0.4}TiO_3$ Bulk Ceramics and Thin Films for Tunable Microwave Applications," *J. Appl. Phys.*, **92**, 3941–6 (2002).
[6]H. Y. Tian, J. Q. Qi, Y. Wang, J. Wang, H. L. W. Chan, and C. L. Choy, "Core-Shell Structure of Nanoscaled $Ba_{0.5}Sr_{0.5}TiO_3$ Self-Wrapped by MgO Derived from a Direct Solution Synthesis at Room Temperature," *Nanotechnology*, **16**, 47–52 (2005).
[7]A. I. Dedyk, E. A. Nenasheva, A. D. Kanareykin, J. V. Pavlova, O. V. Sinjukova, and S. F. Karmanenko, "Tunability and Leakage Currents of (Ba,Sr)TiO_3 Ferroelectric Ceramics with Various Additives," *J. Electroceram.*, **17**, 433–7 (2006).
[8]H. F. Zhang, S. W. Or, and H. L. W. Chan, "Synthesis of Fine-Crystalline $Ba_{0.6}Sr_{0.4}TiO_3$–MgO Ceramics by Novel Hybrid Processing Route," *J. Phys. Chem. Solids*, **70**, 1218–22 (2009).
[9]E. A. Nenasheva, N. F. Kartenko, I. M. Gaidamaka, O. N. Trubitsyna, S. S. Redozubov, A. I. Dedyke, and A. D. Kanareykin, "Low Loss Microwave Ferroelectric Ceramics for High Power Tunable Devices," *J. Eur. Ceram. Soc.*, **30**, 395–400 (2010).
[10]J. J. Zhang, J. W. Zhai, and X. Yao, "Dielectric Tunable Properties of Low-Loss $Ba_{0.4}Sr_{0.6}Ti_{1-y}Mn_yO_3$ Ceramics," *Scripta Mater.*, **61**, 764–7 (2009).
[11]J. J. Zhang, J. W. Zhai, M. W. Zhang, P. Qi, X. Yu, and X. Yao, "Structure-Dielectric Properties Relationship in Mg-Mn Co-Doped $Ba_{0.4}Sr_{0.6}TiO_3$/$MgAl_2O_4$ Tunable Microwave Composite Materials," *J. Phys. D Appl. Phys.*, **42**, 075414 (6pp) (2009).
[12]C. X. Yang, H. Q. Zhou, M. Liu, and T. Qiu, "Effect of $MnCO_3$ Doping on the Dielectric and Tunable Properties of BSTO/MgO Composite for Phase Array Antennas," *J. Mater. Sci. Mater. Electron.*, **18**, 985–9 (2007).
[13]S. F. Wang, Y. C. Hsu, J. P. Chu, and C. H. Wu, "Hexagonal Ba$(Ti_{1-x}Mn_x)O_3$ Ceramics: Microstructural Evolution and Microwave Dielectric Properties," *Appl. Phys. Lett.*, **88**, 042909 (3pp) (2006).

[14]C. Berbecaru, H. V. Alexandru, C. Porosnicu, A. Velea, A. Ioachim, L. Nedelcu, and M. Toacsan, "Ceramic Materials $Ba_{1-x}Sr_xTiO_3$ for Electronics –Synthesis and Characterization," *Thin Solid Films*, **516**, 8210–4 (2008).

[15]H. T. Langhammer, T. Müller, K. H. Felgner, and H. P. Abicht, "Influence of Strontium on Manganese-Doped Barium Titanate Ceramics," *Mat. Lett*., **42**, 21–4 (2000).

[16]B. W. Hakki and P. D. Coleman, "A Dielectric Resonator Method of Measuring Inductive Capacities in the Millimeter Range," *IRE Trans. Microw. Theory Tech*., **8**, 402–10 (1960).

[17]C. Elissalde, C. Estournès, and M. Maglione, "Tailoring Dielectric Properties of Multilayer Composites Using Spark Plasma Sintering," *J. Am. Ceram. Soc*., **90**, 973–6 (2007).

[18]U. C. Chung, C. Elissalde, C. Estournès, M. Paté, J. P. Ganne, and M. Maglione, "Low–Losses, Highly Tunable $Ba_{0.6}Sr_{0.4}TiO_3$/MgO Composite," *Appl. Phys. Lett*., **92**, 042902 (3pp) (2008).

[19]Q. Xu, X. F. Zhang, Y. H. Huang, W. Chen, H. X. Liu, M. Chen, and B. H. Kim, "Effect of MgO on Structure and Non Linear Dielectric Properties of $Ba_{0.4}Sr_{0.6}TiO_3$/MgO Composite Ceramics Prepared from Superfine Powders," *J. Alloys Compd*., **488**, 448–53 (2009).

[20]S. Agrawal, R. Guo, D. Agrawal, A. S. Bhalla, R. R. Neurgaonkar, and C. B. Murray, "Dielectric Tunability of BST:MgO Composites Prepared Using Nano Particles," *Ferroelectr. Lett*., **31**, 149–56 (2004).

[21]F. Batllo, E. Duverger, J. C. Jules, J. C. Niepce, B. Jannot, and M. Maglione, "Dielectric and E.P.R. Studies of Mn- Doped Barium Titanate," *Ferroelectrics*, **109**, 113–8 (1990).

[22]T. Mitsui, *Landolt Börnstein Tables*, Vol. 3. Spinger-Verlag, Berlin, Germany, 1969.

[23]O. G. Vendik and S. P. Zubko, "Ferroelectric Phase Transition and Maximum Dielectric Permittivity of Displacement Type ferroelectrics ($Ba_xSr_{1-x}TiO_3$)," *J. Appl. Phys*., **88**, 5343–50 (2000).

[24]A. Tkach, P. Vilarinho, and A. Kholkin, "Structure-Microstructure-Dielectric Tunability Relationship in Mn-Doped Strontium Titanate Ceramics," *Acta Mater*., **53**, 5061–9 (2005).

[25]V. Hornebecq, C. Huber, M. Maglione, M. Antonietti, and C. Elissalde, "Dielectric Properties of Pure $(BaSr)TiO_3$ and Composites with Different Grain Size: From Nanometer to Micrometer," *Adv. Funct. Mater*., **14**, 899–904 (2004).

[26]Z. Zhao, V. Buscaglia, M. Viviani, M. T. Buscaglia, L. Mitoseriu, A. Testino, M. Nygren, M. Johnsson, and P. Nanni, "Grain Size Effects on the Ferroelectric Behavior of Dense Nanocrystalline $BaTiO_3$ Ceramics," *Phys. Rev. B*, **70**, 024107 (8pp) (2004).

[27]R. A. Serway, W. Berlinger, K. A. Muller, and R. W. Collins, "Electron Paramagnetic Resonance of Three Manganese Centers in Reduced $SrTiO_3$," *Phys. Rev. B*, **16**, 4761–8 (1977).

[28]K. A. Muller, "Paramagnetic Point and Pair Defects in Oxide Perovskites," *J. Physique*, **42**, 551–7 (1981).

[29]V. V. Laguta, A. M. Slipenyuk, I. P. Bykov, M. D. Glinchuk, D. Michau, and M. Maglione, "Electron Spin Resonance Investigation of Impurity and Intrinsic Defects in Nb-Doped $BaTiO_3$ Single Crystal and Ceramics," *J. Appl. Phys*., **97**, 073707 (6pp) (2005).

[30]A. M. Slipenyuk, M. D. Glinchuk, V. V. Laguta, I. P. Bykov, A. G. Bilous, and O. I. V'yunov, "Impurity and Intrinsic Defects in Barium Titanate Ceramics and Their Influence on PTCR Effect," *Ferroelectrics*, **288**, 243–51 (2003).

[31]A. G. Badalyan, C. B. Azzoni, P. Galinetto, M. C. Mozzati, V. A. Trepakov, M. Savinov, A. Dejneka, L. Jastrabik, and J. Rosa, "Impurity Centers and Host Microstructure in Weakly Doped $SrTiO_3$:Mn Crystals: New Findings," *J. Phy. Confer. Ser. [Funct. Mater. Nanotechnol.]*, **93**, 012012 (8pp) (2007).

[32]V. V. Laguta, A. M. Slipenyuk, I. P. Bykov, M. D. Glinchuk, M. Maglione, D. Michau, J. Rosa, and L. Jastrabik, "Electron Spin Resonance Investigation of Oxygen-Vacancy-Related Defects in $BaTiO_3$ Thin Films," *Appl. Phys. Lett*., **87**, 022903 (3pp) (2005).

[33]A. Artemenko, C. Elissalde, U.-C. Chung, C. Estournès, S. Mornet, I. Bykov, and M. Maglione, "Linking Hopping Conductivity to Giant Dielectric Permittivity in Oxides," *Appl. Phys. Lett*., **97**, 1329011–3 (2010).

[34]M. D. Glinchuk, I. V. Kondakova, V. V. Laguta, A. M. Slipenyuk, and I. P. Bykov, "Size Effects in Radiospectroscopy Spectra of Ferroelectric Nanopowders," *Acta Phys. Pol. A*, **108**, 47–60 (2005).

[35]M. D. Glinchuk, A. N. Morozovska, A. M. Slipenyuk, and I. P. Bykov, "Peculiarities of the Radiospectroscopy Line Shape in Nanomaterials," *Appl. Mag. Reson*., **24**, 333–42 (2003).

[36]A. M. Slipenyuk, I. V. Kondakova, M. D. Glinchuk, and V. V. Laguta, "Investigation of Ferroelectric Nanopowders by EPR Method," *Phys. Status Solidi C*, **4**, 1297–300 (2007). □